Infrared Physics & Technology 54 (2011) 382–394

Contents lists available at ScienceDirect

Infrared Physics & Technology

journal homepage: www.elsevier.com/locate/infrared

Adaptive image enhancement based on clustering of wavelet coefficients for infrared sea surveillance systems

A. Onur Karalı [a], O. Erman Okman [b], Tayfun Aytaç [a,*]

[a] TÜBİTAK BİLGEM UEKAE/İLTAREN, Şehit Yzb. İlhan Tan Kışlası, 2432 cad., 2489 sok., TR-06800, Ümitköy, Ankara, Turkey
[b] Department of Electrical and Electronics Engineering, Middle East Technical University, İnönü Blv., TR-06531, Ankara, Turkey

ARTICLE INFO

Article history:
Received 23 November 2010
Available online 27 May 2011

Keywords:
Image enhancement
Imaging infrared systems
Feature extraction
Clustering of wavelet coefficients
Target detection
Sea surveillance systems

ABSTRACT

Most of the techniques developed for infrared (IR) image enhancement (IE) depend heavily on the scene, environmental conditions, and the properties of the imaging system. So, with a set of predefined scenario properties, a content-based IR-IE technique can be developed for better situational awareness. This study proposes an adaptive IR-IE technique based on clustering of wavelet coefficients of an image for sea surveillance systems. Discrete wavelet transform (DWT) of an image is computed and feature vectors are constructed from subband images. Clustering operation is applied to group similar feature vectors that belong to different scene components such as target or background. Depending on the feature vectors, a weight is assigned to each cluster and these weights are used to compute gain matrices which are used to multiply wavelet coefficients for the enhancement of the original image. Enhancement results are presented and a comparison of the performance of the proposed algorithm is given through subjective tests with other well known frequency and histogram based enhancement techniques. The proposed algorithm outperforms previous ones in the truthfulness, detail visibility of the target, artificiality, and total quality criteria, while providing an acceptable computational load.

1. Introduction

An IR image of a sea-surface scene includes the effects due to the sky reflections, sun glints, blackbody emissions from the wave facets, and atmosphere [1], which decrease the visibility of the target details. Sensor noises and thermodynamic state of the targets are also crucial for detection and identification of the targets in the sea background or at the horizon. Therefore, for a better visualization of high dynamic range (HDR) IR images containing sea-surface targets, it is vital to develop IE techniques that increase the contrast between the target and background as well as emphasize target edges and texture.

Many of the surveillance systems such as IR search and track systems require intruder detection, threat detection approaching from sea or horizon, and better visualization of extended targets for classification and identification purposes. Infrared IE is important in these applications where enhanced target details give more cues about the target type and increase situational awareness in man-in-the-loop systems. The main motivation in developing content based IE technique is that the proposed solutions for enhancement are case dependent and it is very difficult to develop an enhancement technique working well under different conditions. By intelligently developing algorithms and adjusting their internal parameters for specific applications as in the sea surveillance case, it is possible to develop more efficient enhancement techniques.

Application of the DWT for IE gives us an opportunity for detecting anomalies in a scene with spatial information. By extracting and examining these anomalies carefully, the scene can be divided into regions and a spatially varying enhancement of the image can be achieved. Target edges and texture can be enhanced independent of the clutter and the noise in the background region. We propose an adaptive IR-IE technique based on clustering of wavelet coefficients of the image for sea surveillance systems. To the best of our knowledge, no attempt has been previously made to develop an IR-IE technique in wavelet domain specific for sea-surface targets and to compare its performance with other enhancement methods. We show through subjective tests that it performs well in the truthfulness, detail visibility of the target, artificiality, and total quality criteria when compared to other histogram and frequency based enhancement methods.

This paper is organized as follows: Section 2 provides a brief review about IR-IE techniques. In Section 3, the proposed algorithm is explained. Experimental results with a detailed discussion of the effects of the algorithm parameters on the performance are provided in Section 4. Subjective comparisons and computational

* Corresponding author. Tel.: +90 312 291 6051; fax: +90 312 291 6004.
E-mail addresses: onur.karali@iltaren.tubitak.gov.tr (A.O. Karalı), eokman@eee.metu.edu.tr (O.E. Okman), tayfun.aytac@iltaren.tubitak.gov.tr (T. Aytaç).

1350-4495/$ - see front matter © 2011 Elsevier B.V. All rights reserved.
doi:10.1016/j.infrared.2011.05.003

cost of the algorithms are presented in Section 5. Concluding remarks are made and directions for future research are provided in the last section.

2. Related work

Image enhancement techniques are generally divided into four categories, which are amplitude scaling, histogram modification, noise removal, and edge enhancement [2]. Local area processing method based on histogram shaping and adaptive Wiener filtering for noise removal are used together for contrast enhancement in [3]. In [4], edges are enhanced by adaptive thresholding using error-diffusion algorithm. The authors implemented a spatiotemporal homomorphic filtering technique using a qualitative model for the far IR scenes in [5,6]. Infrared images are enhanced using autoregressive moving average filter and H_∞ bounds in [7]. In [8], anomalous frequency is detected using Fourier transform along the column in image block and inverse Fourier transform is applied to the thresholded frequency for enhancement. Balanced contrast limited adaptive histogram equalization and contrast enhancement (BCLAHE-CE) techniques are used together for improved visualization of IR images in [9]. Evaluation is performed through subjective analysis based on human observers. It outperforms histogram equalization, Fattal's method [10], and retinex algorithm [11] in the subjective tests. In [12], bilateral filter is used for the dynamic range compression of IR HDR images and the proposed algorithm is compared with histogram equalization and retinex algorithms [11]. An adaptive contrast IR enhancement method is proposed in [13] which uses a quantitative model and adaptive plateau histogram equalization. For long range IR surveillance purposes, adaptive histogram equalization and high-boost filters are used together in [14]. For the same purpose, hit-or-miss transform based morphological approach is proposed in [15]. Multiscale top-hat transform is used in contrast enhancement in [16] and the performance is compared with histogram and morphological based approaches using fuzziness index for sea and sky backgrounds. IR-IE based on human visual system is proposed in [17] using multifractal theory. A novel unsharp masking algorithm is presented in [18], where contrast and sharpness are controlled by the user and halo effects are reduced using edge-preserving filters. In [19], after constrained histogram equalization, unsharp masking is applied for contrast and edge enhancement.

The wavelet transform has been widely used for texture segmentation [20] and face [21], fingerprint [22], and mammogram enhancement [23]. In [24], a wavelet-based dynamic range compression algorithm is proposed for aerial images. Wavelet based histogram equalization method is developed in [25]. Directional wavelets and image gradients are used together in [26]. A two-stage IR-IE technique based on local and global contrast enhancement is proposed in [27]. The authors first enhance global contrast by adaptive plateau histogram equalization and then use adaptive gain control based on wavelet transform for local contrast enhancement. In [28], an adaptive contrast enhancement method based on wavelet transform is proposed. At each sublevel, horizontal and vertical images are added and zero-crossing points are found that are close to the segmented regions. At each scale, the boundary map is blurred with a Gaussian filter. This map is used as a weight in the enhancement of horizontal, vertical, and diagonal subband images. Discrete stationary wavelet transform is used with genetic algorithm for typhoon cloud IE in [29].

In our previous work [30], we proposed an adaptive enhancement method based on local frequency cues (AEMLFC) for sea-surface targets. The image is transformed blockwise into Fourier domain and clustering is done according to the number of expected regions to be enhanced in the scene. Based on the variations of the elements in any cluster and the differences between the cluster centers in frequency domain, two gain matrices are computed for mid and high frequency components of the image which are used in the construction of the enhanced image. We showed through subjective and quantitative tests that it performs well for the detail visibility in the target region when compared to histogram [9,27,31] and unsharp masking based methods [32]. In this study, we develop an adaptive enhancement method based on clustering of wavelet coefficients (AEMCWC). The work is different from [30] in a way that the proposed approach clusters wavelet coefficients to find regions to be enhanced and uses the relation between the subband images to find gains used in the reconstruction step. Another difference is that both clustering and enhancement operations are implemented in the wavelet domain, which makes the proposed method more robust when compared to that in our previous work where operations are implemented both in the spatial and frequency domain.

3. Image enhancement by clustering of wavelet coefficients

An example IR image taken from a ground based sea surveillance system and its histogram are shown in Fig. 1a and b, respectively. As shown in Fig. 1b, the histogram has a two modal distribution, where the first and second parts correspond to the background, i.e., sea and sky region, respectively. These two parts have intensity values ranging approximately between [16,000, 17,000] and [17,000, 17,600], respectively. A typical scene consists of sea surface with wave glints, sky with gradual distribution, small islands, and targets. Wavelet coefficients are used to detect these scene components and discriminate the target from the background. Our aim is to enhance the image by multiplying the wavelet coefficients with gain factors without introducing artifacts. The summary of the proposed algorithm, which is detailed in the following sections, is given in Table 1.

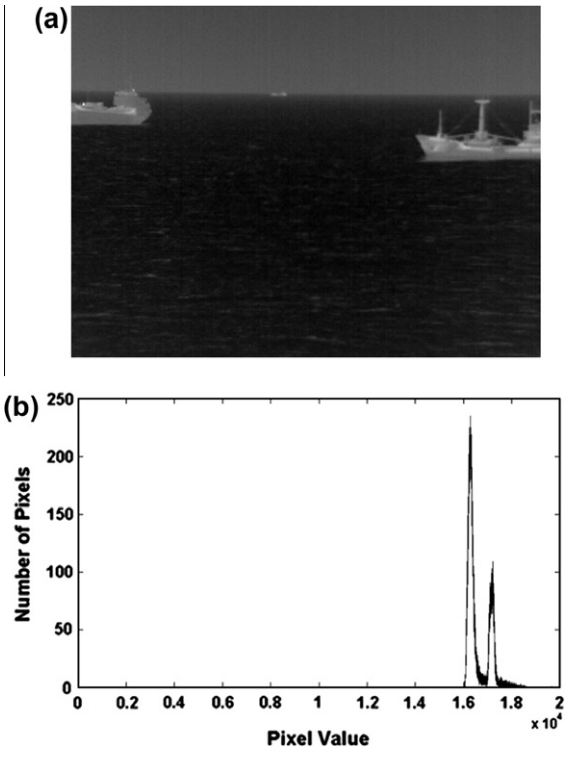

Fig. 1. (a) Sample image and (b) its histogram.

Table 1
Summary of the proposed method.

Step 1	Decompose the original image by DWT
Step 2	Cluster wavelet coefficients to group similar feature vectors
Step 3	Assign weights to each cluster and compute weight matrices
Step 4	Compute gain matrices from the weight matrices
Step 5	Multiply each subband image with the appropriate gain matrix
Step 6	Reconstruct the new wavelet coefficients by IDWT to obtain enhanced image

3.1. Discrete wavelet transform

The main idea behind DWT is to split a signal into components according to the frequency spectrum of the signal while preserving its spatial structure. For instance, DWT splits a signal into two parts, the low and high frequency components. The edges in the signal are generally confined in the high frequency part. The low frequency part is then split into two parts again and again until the signal is entirely decomposed or the desired level of decomposition is obtained. The original signal can be obtained from the decomposition outputs and this process is called inverse DWT (IDWT).

A signal $X(n)$ can be decomposed into its low and high frequency components as follows:

$$f_{low}(m) = \sum_n g(2m-n)\cdot X(n), \tag{1}$$

$$f_{high}(m) = \sum_n h(2m-n)\cdot X(n). \tag{2}$$

The low pass (g) and high pass (h) filters satisfy the condition $g[N-1-n] = (-1)^n \cdot h(n)$ for the orthogonal quadrature mirror filter banks, where N is the filter length. f_{low} and f_{high} are the approximation and detail coefficients of the image, respectively. Furthermore, the IDWT is obtained by recursively obtaining the low frequency components as follows:

$$X(n) = \sum_m g'(2m-n)\cdot f_{low}(m) + \sum_m h'(2m-n)\cdot f_{high}(m), \tag{3}$$

where g' and h' are the reconstruction filters.

The two-dimensional (2-D) DWT or IDWT for an image is defined similarly by evaluating the one-dimensional DWT or IDWT for each dimension separately. One level decomposition and reconstruction along the rows and columns are given in Fig. 2. The subband images at different levels are obtained by applying the same procedure to the approximation image (I_{LL}) successively. The subband images I_{LH}, I_{HL}, and I_{HH} represent the vertical, horizontal, and diagonal details, respectively.

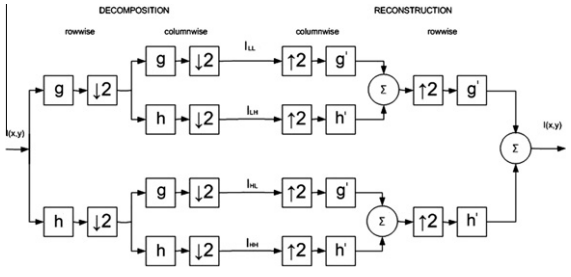

Fig. 2. One level wavelet decomposition and reconstruction.

3.2. Clustering in wavelet domain

In this work, P levels of wavelet coefficients of the HDR IR image are computed. P should be determined with respect to the frame size of the imaging system and the total number of pixels that the target spans. For the sample image given in Fig. 1a, the subband images can be seen in Fig. 3 at different decomposition levels k, ranging from 1 to P. As seen in the figure, vertical $\left(I_k^{LH}\right)$ and diagonal $\left(I_k^{HH}\right)$ details reveal the boundaries of the extended target edges, whereas edges in the sea surface and the horizon can be seen clearly in the horizontal details $\left(I_k^{HL}\right)$. Region pyramids are defined over these k levels of wavelet coefficients and a feature vector is defined for each region pyramid. Entries of the feature vector are computed from the wavelet coefficients that are inside the regions of the corresponding region pyramid. Similar feature vectors are grouped to differentiate scene components such as target and background.

First of all, the P levels wavelet coefficients of the image are evaluated and normalized wavelet coefficients are obtained using below equation:

$$\underline{I_k^s(x,y)} = \frac{\left|I_k^s(x,y)\right|}{\sum_x\sum_y\left|I_k^s(x,y)\right|}, \tag{4}$$

where $\underline{I_k^s(x,y)}$ represents the normalized wavelet coefficient of the kth level subband image at the indices x and y and s denotes the type of the subband image and is a member of the set {LL, LH, HL, HH}.

Secondly, region pyramids are computed for each pixel of the Pth level approximation image. The idea behind the region pyramid is that each wavelet coefficient in the kth level subband image is computed as a linear combination of wavelet coefficients inside a region in the $(k-1)$st level approximation image. This region is denoted as R_{k-1}. So, for a single pixel in the Pth level approximation image, we can compute a region pyramid as seen in Fig. 4. In this figure, center coordinates of R_l are defined as x_l and y_l; width and height of the region R_l are defined as w_l and h_l, where l takes the values $\{P-1,\ldots,1\}$. Calculation of the parameters of each region in the pyramid that is defined for the pixel at (x, y) of $\underline{I_P^{LL}}$ is done by using following equations:

$$w_l = 2\cdot w_{l+1} + N - 2, \tag{5}$$

$$h_l = 2\cdot h_{l+1} + N - 2, \tag{6}$$

$$x_l = 2\cdot x_{l+1} - \frac{N}{2} + 1, \tag{7}$$

$$y_l = 2\cdot y_{l+1} - \frac{N}{2} + 1. \tag{8}$$

where N is the size of the wavelet filter. Parameters of regions in the pyramid are calculated step by step as l goes from $P-1$ to 1. For $l = P$, w_P and h_P are equal to 1. Calculation is completed when the parameters of R_1 are computed and a region pyramid that consists of P layers is obtained for all (x, y) in the Pth level approximation image.

At the next step, a feature vector F is constructed for each region pyramid which consists of $3P + 1$ entries. The first entry of this vector, f_1 is the corresponding normalized wavelet coefficient evaluated using the Pth level approximation image. The remaining elements of this vector is evaluated by the following equations:

$$f_{3m+2} = \frac{1}{w_{P-m}\cdot h_{P-m}} \sum_{(x,y)\in R_{P-m}} \underline{I_{P-m}^{LH}(x,y)}, \tag{9}$$

$$f_{3m+3} = \frac{1}{w_{P-m}\cdot h_{P-m}} \sum_{(x,y)\in R_{P-m}} \underline{I_{P-m}^{HL}(x,y)}, \tag{10}$$

$$f_{3m+4} = \frac{1}{w_{P-m}\cdot h_{P-m}} \sum_{(x,y)\in R_{P-m}} \underline{I_{P-m}^{HH}(x,y)}, \tag{11}$$

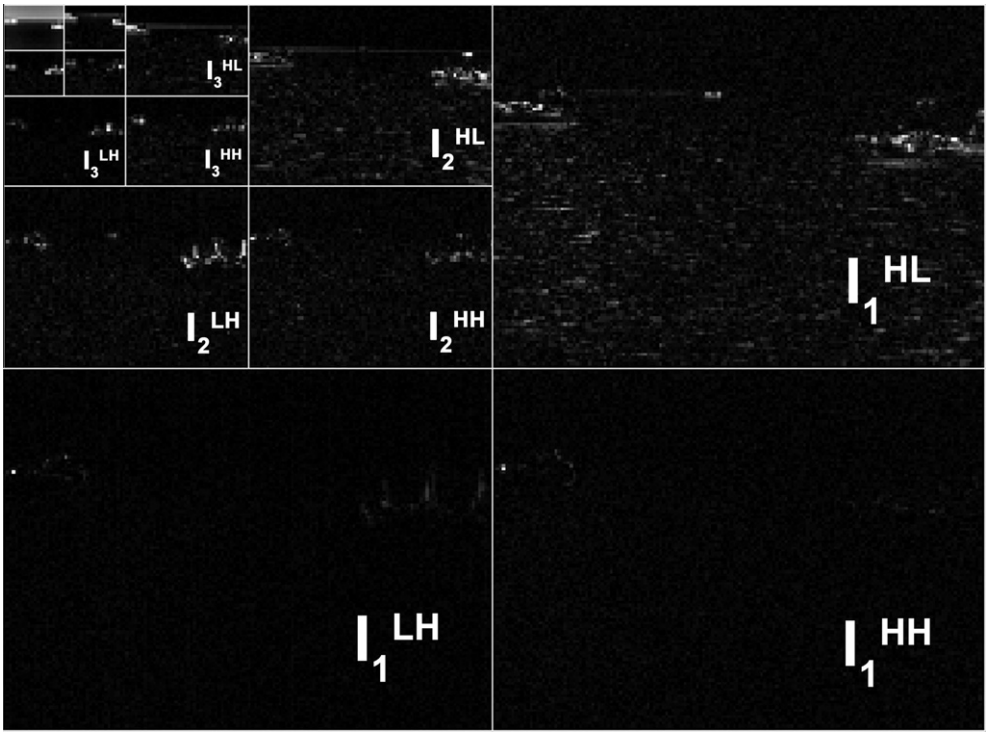

Fig. 3. Four level subband images obtained by Daubechies-3 wavelet filters for the sample image shown in Fig. 1a.

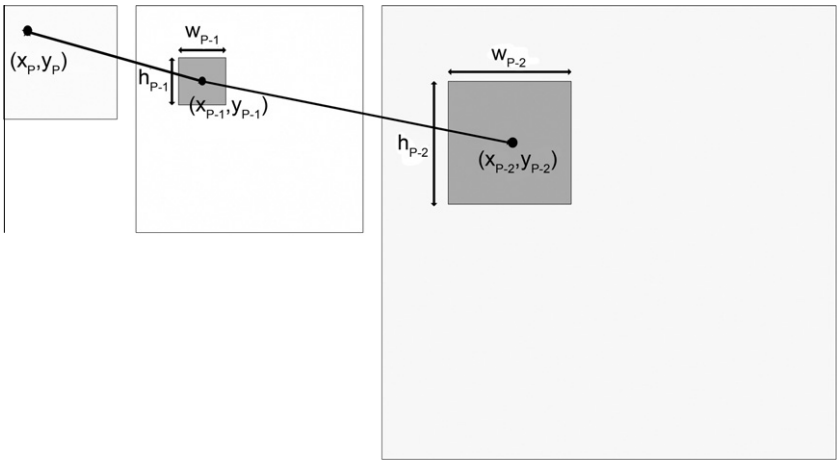

Fig. 4. Regions R_{P-1} and R_{P-2} used in extraction of feature vectors.

where m takes values ranging from 0 to $P-1$. As seen from the equations above, the entries of the feature vectors are the average of the appropriate set of wavelet coefficients. Four feature vectors computed from four level of wavelet coefficients corresponding to the labeled parts in Fig. 5 are shown in Fig. 6. It can be clearly seen that the four components of the scene have different attributes. This fact is our main motivation in clustering these feature vectors and defining possible target and background regions for further enhancement.

Because the feature vectors are computed for each pixel of the Pth level approximation image of size A_P by B_P, we have $A_P \times B_P$ feature vectors. The next step is to cluster these vectors. Hierarchical cluster tree is obtained using the distances in between the feature vectors and clustering is done with respect to the nearest distance [33]. The distance between two feature vectors is defined as:

$$d_{rs}^2 = (F_r - F_s)(F_r - F_s)^T, \tag{12}$$

where r and s are integers changing from one to $A_P \times B_P$.

For each cluster, more than one centroid may be computed and different weights may be assigned to centroids in each cluster. In our trials, this does not make great difference when compared to assigning weights to a single cluster centroid. Therefore, cluster centers are computed by averaging the elements of each cluster and a weight is calculated for each cluster center. ith entry of each cluster center is normalized with respect to the minimum value of ith entry of all cluster centers and proportional cluster centers (PCC vectors) are obtained as below:

$$PCC_o(i) = \frac{CC_o(i)}{min[\,CC_1(i) \quad CC_2(i) \quad \ldots \quad CC_c(i)\,]}, \tag{13}$$

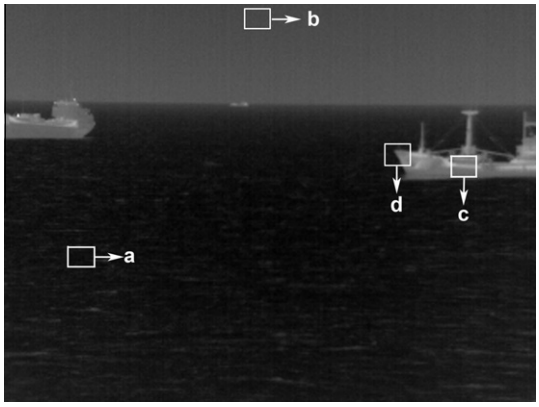

Fig. 5. Sample IR scene. Blocks indicate different scene components: (a) sea, (b) sky, (c) target, and (d) target-sea transition.

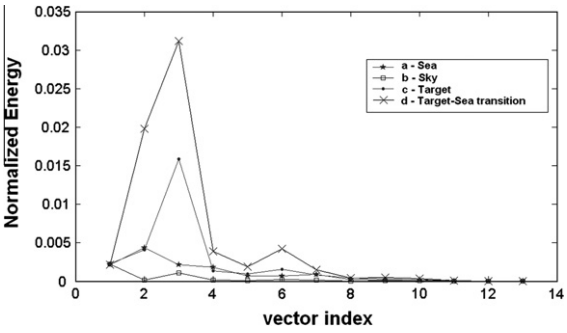

Fig. 6. Feature vectors for the different scene components seen in Fig. 5.

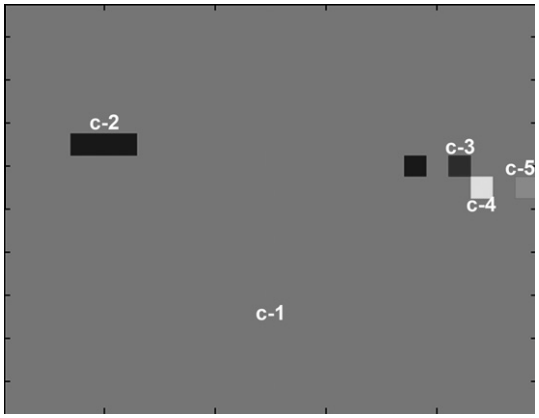

Fig. 7. Clusters found for $c = 5$.

where CC_o is the oth cluster center and i is changing from 1 to $3P+1$. Computed CC and PCC vectors for the image given in Fig. 1a can be seen in Fig. 8. Difference between the CC and PCC can be observed clearly, especially at the latter entries of the cluster centers.

Finally, weights assigned to each cluster, λ_o are obtained by computing the mean value of the proportional cluster center as given in Eq. (14).

$$\lambda_o = \frac{1}{3P+1}\sum_{i=1}^{3P+1} PCC_o(i). \tag{14}$$

Weight matrices are constructed using these weights, which will be explained in more detail in the following subsection.

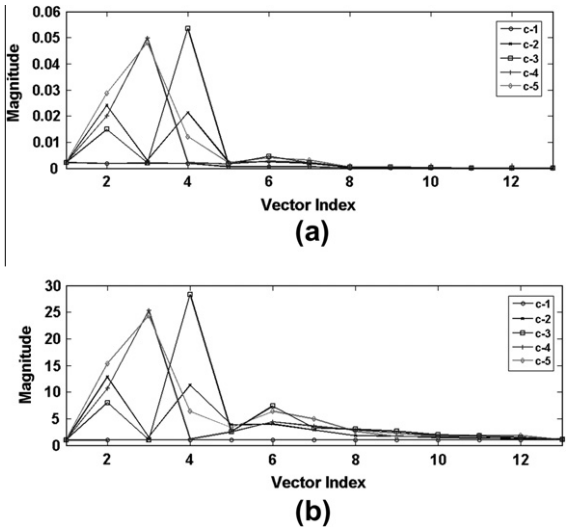

Fig. 8. (a) Cluster centers and (b) proportional cluster centers.

3.3. Enhancement

In the enhancement step, first of all, we define a weight matrix Λ_P of size $A_P \times B_P$ which is determined using the weights λ_o explained in the previous section. For each element of Λ_P, a region pyramid is defined as in Section 3.2 over this weight matrix pyramid and the entries inside the volume defined by this region pyramid are set as the value of the corresponding entry of Λ_P. At the sections where two or more region pyramids, defined for the neighboring elements of Λ_P, overlap, average values of the neighboring elements are assigned to the values of elements in these regions.

Weight matrices computed for each level of the image given in Fig. 1a can be seen in Fig. 9. As seen from this figure, there are peaks in the target regions which give us the ratio between the gain coefficients defined for each scene component. This ratio allows us to enhance the details in the image with different gain coefficients depending on the spatial position. Also, by defining a weight matrix for each of the Pth level subband images, we have the ability to define different gain coefficients for the different detail levels, i.e. different frequency components, even if they are spatially overlapping.

3.3.1. Gain matrix generation

Weight matrices give us cues about the position of the target and the ratios of the inter-cluster gain coefficient distribution. However, we can not directly apply each weight matrix as a gain because target enhancement, noise removal, and background suppression issues require carefully selection of the gain coefficients. So, for each level of the wavelet coefficient, weight matrices of the corresponding level are mapped to different ranges by the following mapping operation:

$$G_k = \frac{(\Lambda_k - min(\Lambda_k))\alpha_k}{(max(\Lambda_k) - min(\Lambda_k))} + \beta_k, \tag{15}$$

where G_k is the gain matrix, α_k defines the dynamic range of the gain coefficient, and β_k is the offset for the kth level. For obtaining smooth transition between detail levels of the target and background regions in the boundaries, a low pass filtering operation over first and second level gain matrices is required. This operation reduces the artificiality of the enhanced image by providing smooth gain coefficient distribution in the boundary regions. An averaging filter is applied for this purpose in our algorithm.

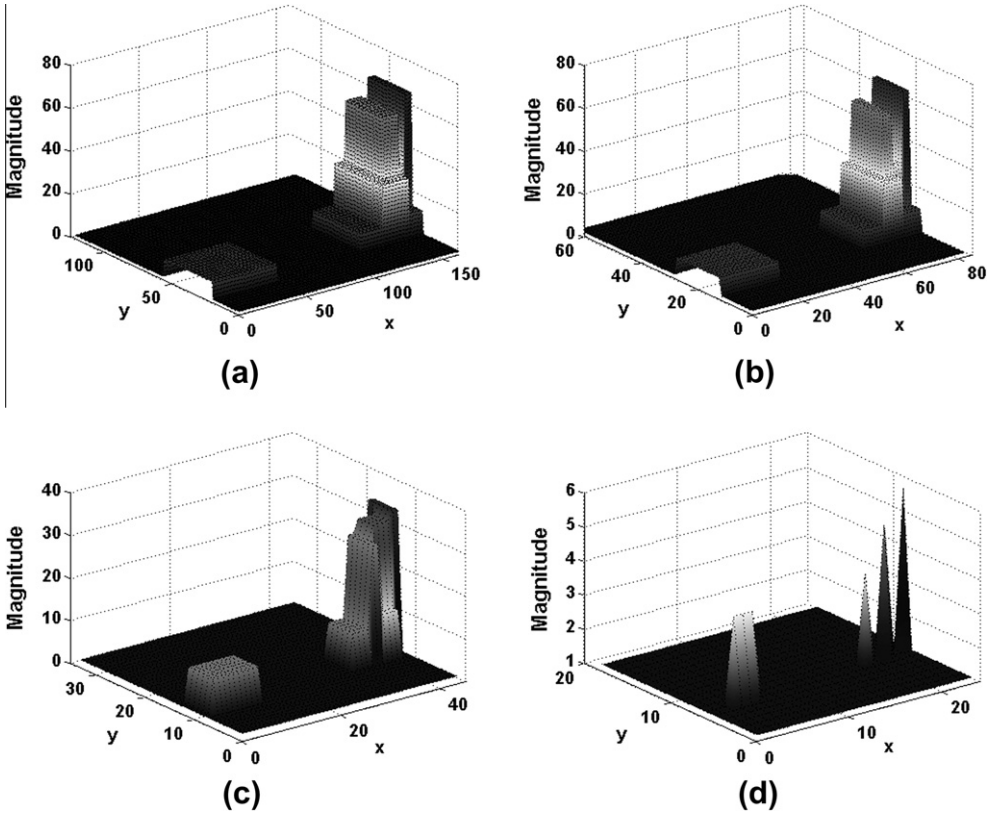

Fig. 9. Weight matrices for the (a) first, (b) second, (c) third, and (d) fourth level subband images.

3.3.2. Image enhancement and reconstruction

After the construction of the gain matrices, kth level horizontal, vertical, and diagonal wavelet coefficients are elementwise multiplied with the G_k to obtain the enhanced coefficients, while approximation coefficients are kept at their original values. Enhanced HDR image is obtained by taking the IDWT of these coefficients. In order to show the original image on the display, a linear mapping function is defined to represent it in 0–255 range and the same mapping function is applied to the enhanced image to display it on the screen. Note that during this mapping, the values outside the 0–255 range are clipped.

4. Experimental results

In this section, we introduce the experimental setup used in obtaining the images, discuss thoroughly the choice of the parameters of the proposed algorithm, and present enhancement results.

Sample images examined in this work are obtained at field trials using two long-wave IR cameras working in $8-12$ μm range. The image sizes extracted from the cameras are [136,272] and [240,320] and the camera is located on ground to observe the scene. Different scenarios include images containing single or multiple targets, targets located at different ranges and orientations, and recorded at different daytimes.

We use Daubechies-3 wavelet filters in computing wavelet coefficients. Four level of wavelet coefficients are found to be suitable in our case to extract sufficient number of feature vectors that have enough discrimination property. A 10×10 averaging filter is selected for smoothing gain matrices. The filter should be sufficiently large to smooth the transitions between the gain matrices and small enough not to remove cluster weights with smaller areas.

Expected number of scene components should be set as the minimum value that the number of maximum clusters c can take. Result of the clustering operation for the sample image given in Fig. 1a, when c is set as 5, can be seen in Fig. 7.

Effect of noise and clutter on wavelet coefficients can be seen in Fig. 3 and from this figure it can be inferred that overenhancement of the first level wavelet coefficients increases the noise level in the background and overenhancement of the second level wavelet coefficients will result in more apparent wave glints in the scene.

The parameters α_k and β_k adjust the variation of the gain coefficients in between target and background regions for the kth level horizontal, vertical, and diagonal wavelet coefficients. α_3 and α_4 are set as 0.1 and β_3 and β_4 are set as one throughout this work because the third and fourth level wavelet coefficients result in saturation in the target region and artifacts appear in the background when they are multiplied with high values.

α_3, α_4, β_3, and β_4 are kept constant throughout trials and slight contrast enhancement is aimed for not saturating the target region. Selection of the parameters α_1, α_2, β_1, and β_2 has more effect on the enhancement and is discussed in detail in the experimental study section.

We examine the selection of α_1, α_2, β_1, and β_2 parameters and see the effect of each parameter on the enhancement of the target region. When α_1 is selected to be high, target edges and details are enhanced as well as the noise in the target region. However, if α_1 is selected to be more than 10, details become saturated and artificiality of the image increases due to the high detail level visibility difference between the target and background regions. The effect of the selection of α_1 on the image can be seen clearly in Fig. 10

for the values of $\alpha_1 = 0$, $\alpha_1 = 5$, and $\alpha_1 = 10$. The parameter α_2 defines the range of values that G_2 will take in case we have a predefined offset value β_2. This parameter defines how much the 2nd level horizontal, vertical, and diagonal wavelet coefficients in the target region will be enhanced. Results obtained for different values of α_2 are shown in Fig. 11. Overenhancement of the second level wavelet coefficients results in halo effects around the target and wave glints around the target region become more apparent where artificiality of the image increases.

As explained before, β_1 is the offset value for the G_1 and selection of the parameter β_1 has effect on the first level detail visibility of the background region. It is selected to be one for the enhancement results given in Fig. 10 to have no enhancement or suppression in the background. In Fig. 12, change in the background detail visibility for different values of β_1 is shown. As mentioned before, 2nd level detail coefficients consist of wave glints and broken clouds in the background region and selection of β_2 affects the visibility of these scene components. Fig. 13 represents the effects of β_2 on the enhancement results.

Selection of the parameter c has effect on the enhancement result since spatial variation of the gain coefficients depends on the regions obtained by clustering operation. Setting the value of c less than 4 usually results in overlapping of target regions with background so undesired enhancement or suppression occurs. Increasing the value of c usually divides the target region into more clusters and smoother transition is achieved from target to background regions by introducing more transition clusters while there is a slight increase in the computation cost. The effect of c on the enhancement results is presented in Fig. 14.

Effect of each parameter on the enhancement result is examined and best results are obtained for the values of α_1, α_2, β_1, β_2, and c to be 4, 1, 1, 1.5, and 20, respectively. With these parameter values, the enhancement results for the different sea surface scenarios are shown in Fig. 15. Results show that the visibility of target edges and texture are enhanced significantly while keeping the noise and clutter in the scene at an acceptable level.

5. Comparative analysis

In this section, the performance and computational cost of the proposed method is compared with other well known techniques. The compared algorithms are selected as AEMLFC, BCLAHE-CE, method of A are Mällo (MAM) [31], and a wavelet based enhancement method (WEM) [34]. The first three methods are chosen because they perform well in the subjective comparisons in our earlier work [30]. The last method is chosen for a fair comparison of the proposed method with another wavelet based method.

The parameters used for the algorithms AEMLFC, BCLAHE-CE, and MAM are explained in detail in [30]. In the WEM, the magnitude of the horizontal and vertical subband images are computed at each pixel position as given below:

$$M(x,y) = \sqrt{\left(I_1^{LH}(x,y)\right)^2 + \left(I_1^{HL}(x,y)\right)^2}. \tag{16}$$

If this value is greater than a threshold value (γ in Eq. (17)), this pixel value is not enhanced to avoid overenhancement. Depending on the M value, pixel values at the horizontal and vertical details are multiplied with different gains and enhanced image is obtained with the reconstruction of the new horizontal and vertical subband images.

$$I_1^s(x,y) = \begin{cases} \left(\frac{\gamma}{n}\right)^p I_1^s(x,y), & M(x,y) \leqslant n, \\ \left(\frac{\gamma}{M(x,y)}\right)^p I_1^s(x,y), & n < M(x,y) \leqslant \gamma, \\ I_1^s(x,y), & M(x,y) > \gamma. \end{cases} \tag{17}$$

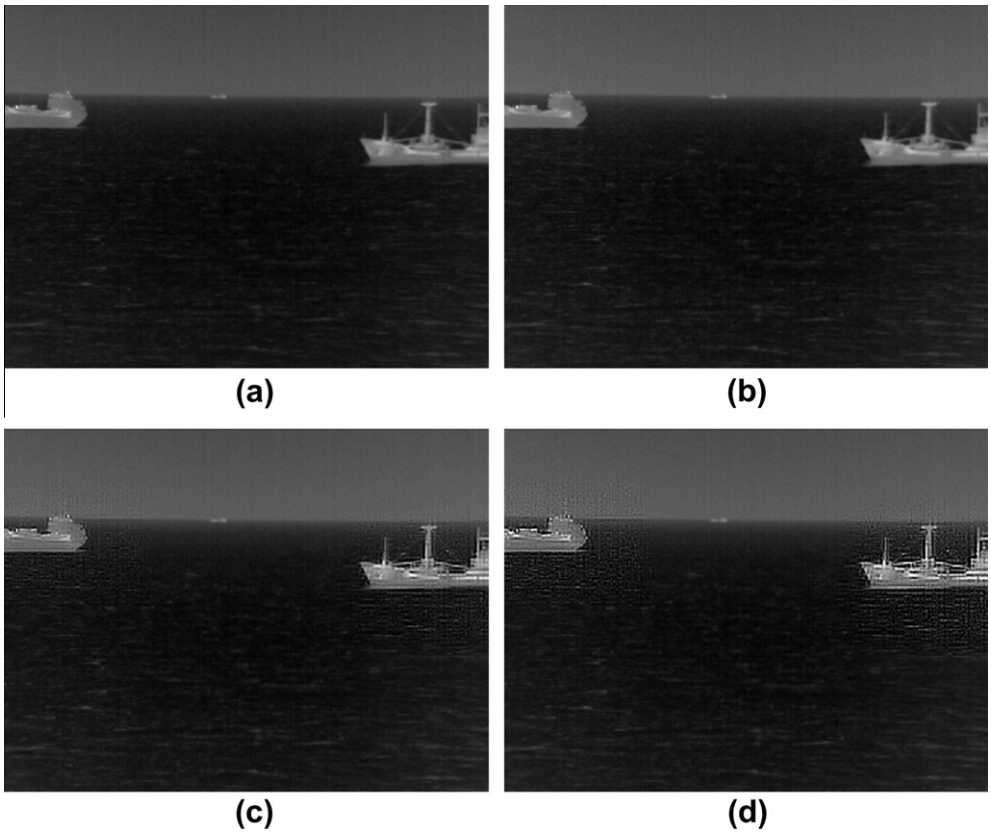

Fig. 10. (a) Original image and enhancement results ($\alpha_2 = 0$, $\beta_1 = 1$, and $\beta_2 = 1$) for: (b) $\alpha_1 = 0$, (c) $\alpha_1 = 5$, and (d) $\alpha_1 = 10$.

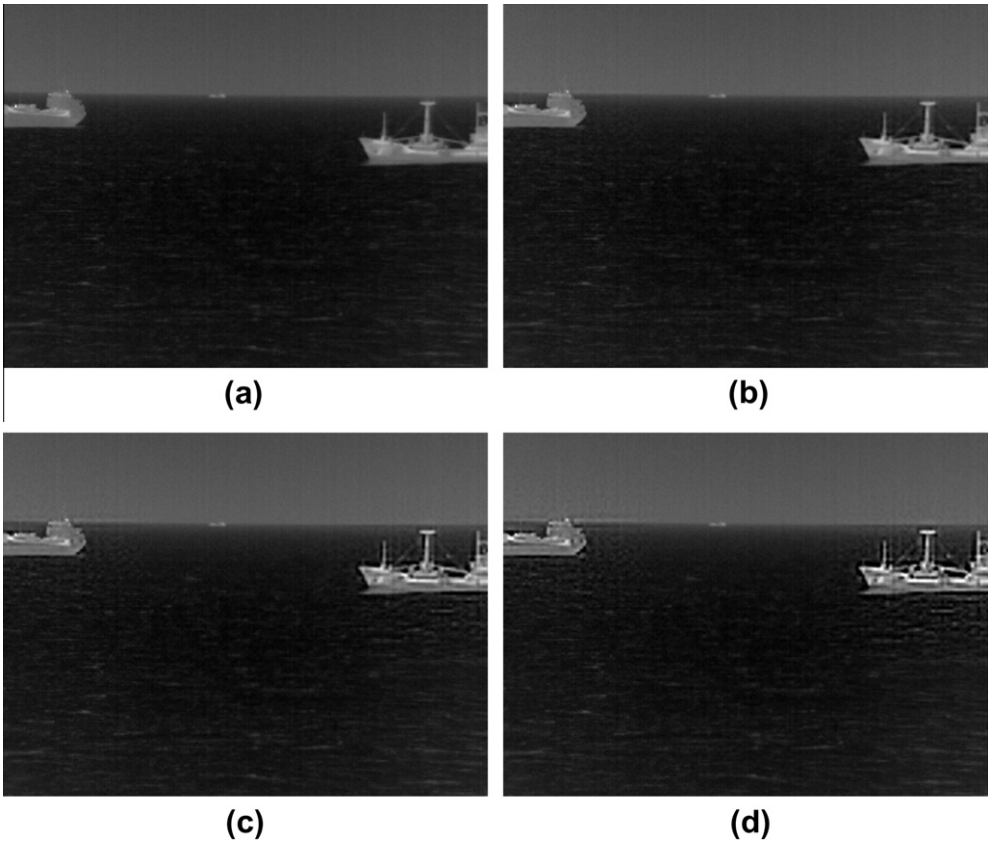

Fig. 11. (a) Original image and enhancement results ($\alpha_1 = 0$, $\beta_1 = 0$, and $\beta_2 = 1$) for: (b) $\alpha_2 = 1$, (c) $\alpha_2 = 3$, and (d) $\alpha_2 = 5$.

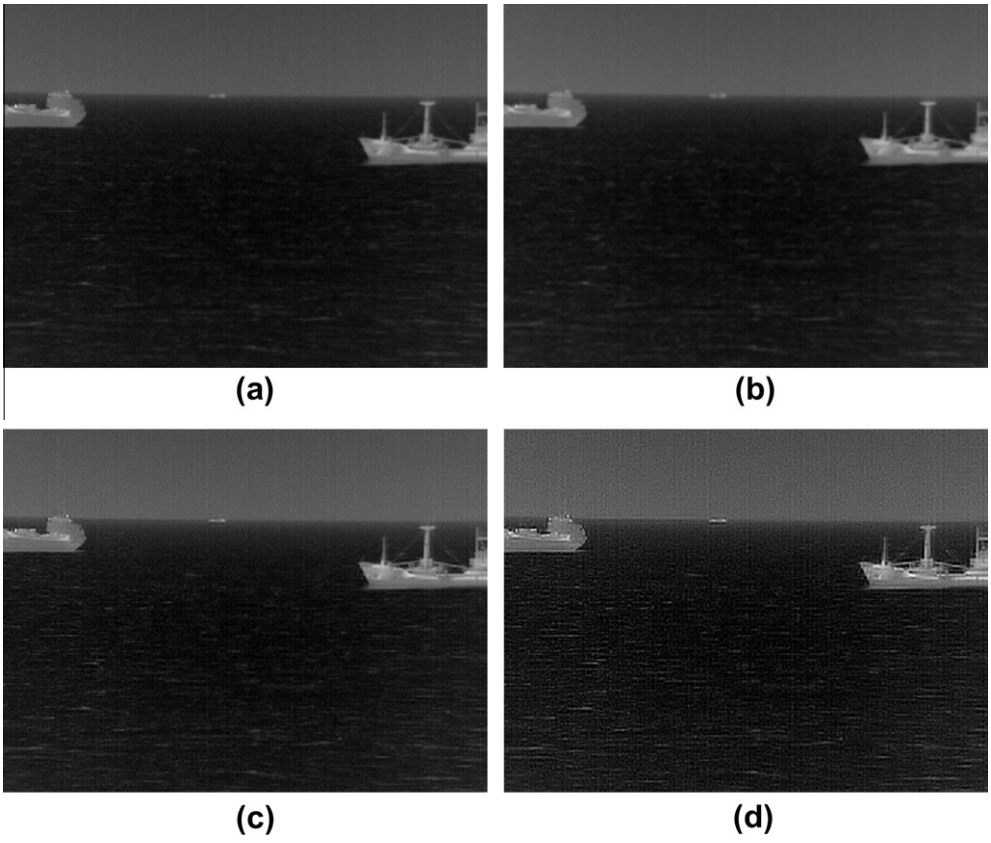

Fig. 12. (a) Original image and enhancement results ($\alpha_1 = 0$, $\alpha_2 = 0$, and $\beta_2 = 1$) for: (b) $\beta_1 = 0.5$, (c) $\beta_1 = 2$, and (d) $\beta_1 = 4$.

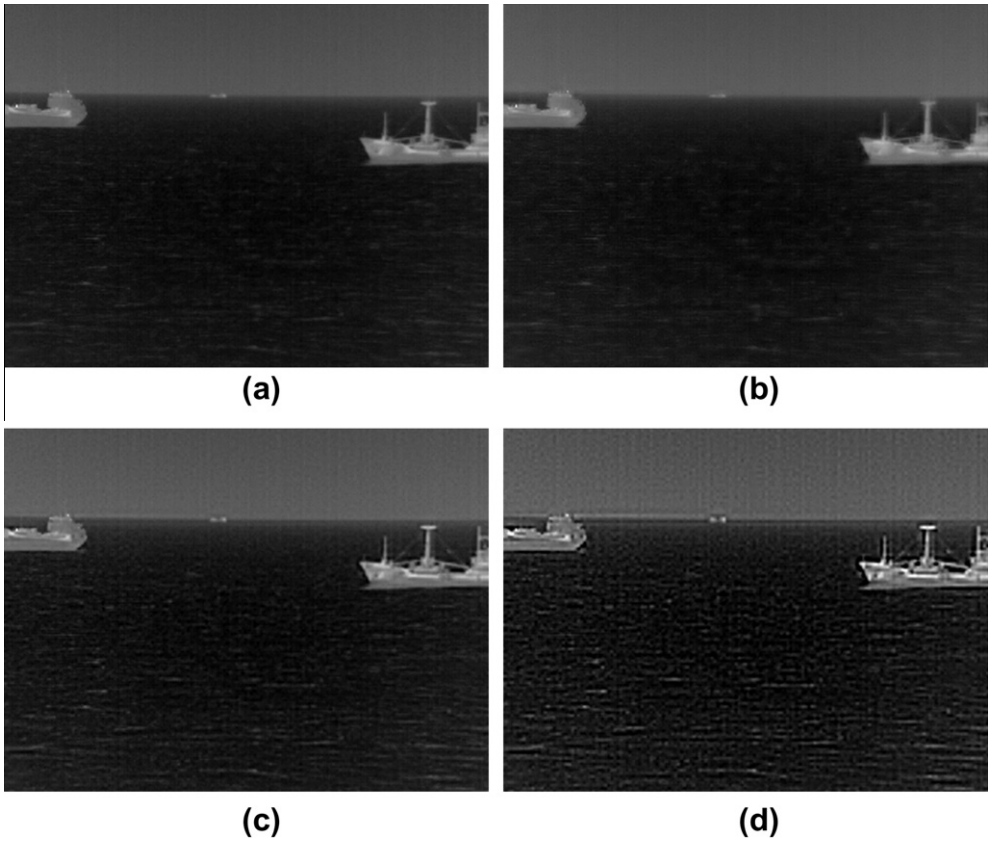

Fig. 13. (a) Original image and enhancement results ($\alpha_1 = 0$, $\alpha_2 = 0$, and $\beta_1 = 1$) for: (b) $\beta_2 = 0.5$, (c) $\beta_2 = 2$, and (d) $\beta_2 = 4$.

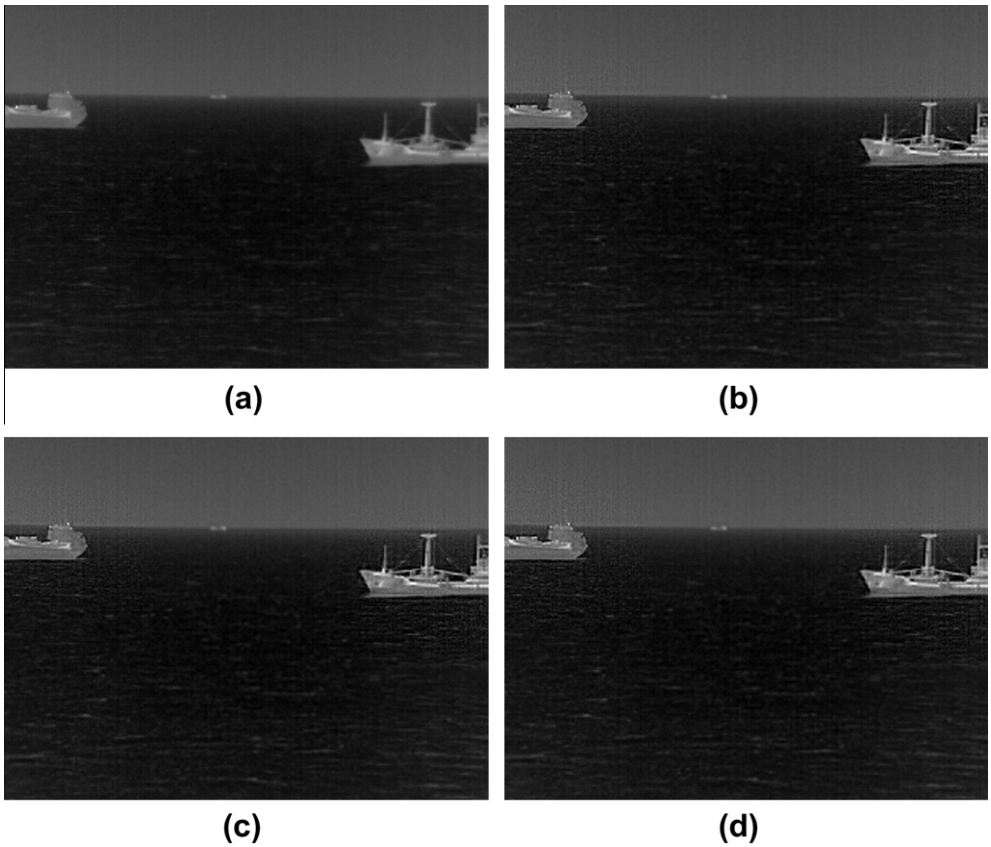

Fig. 14. (a) Original image and enhancement results ($\alpha_1 = 4$, $\alpha_2 = 1$, $\beta_1 = 1$, and $\beta_2 = 1.5$) for: (b) $c = 5$, (c) $c = 10$, and (d) $c = 20$.

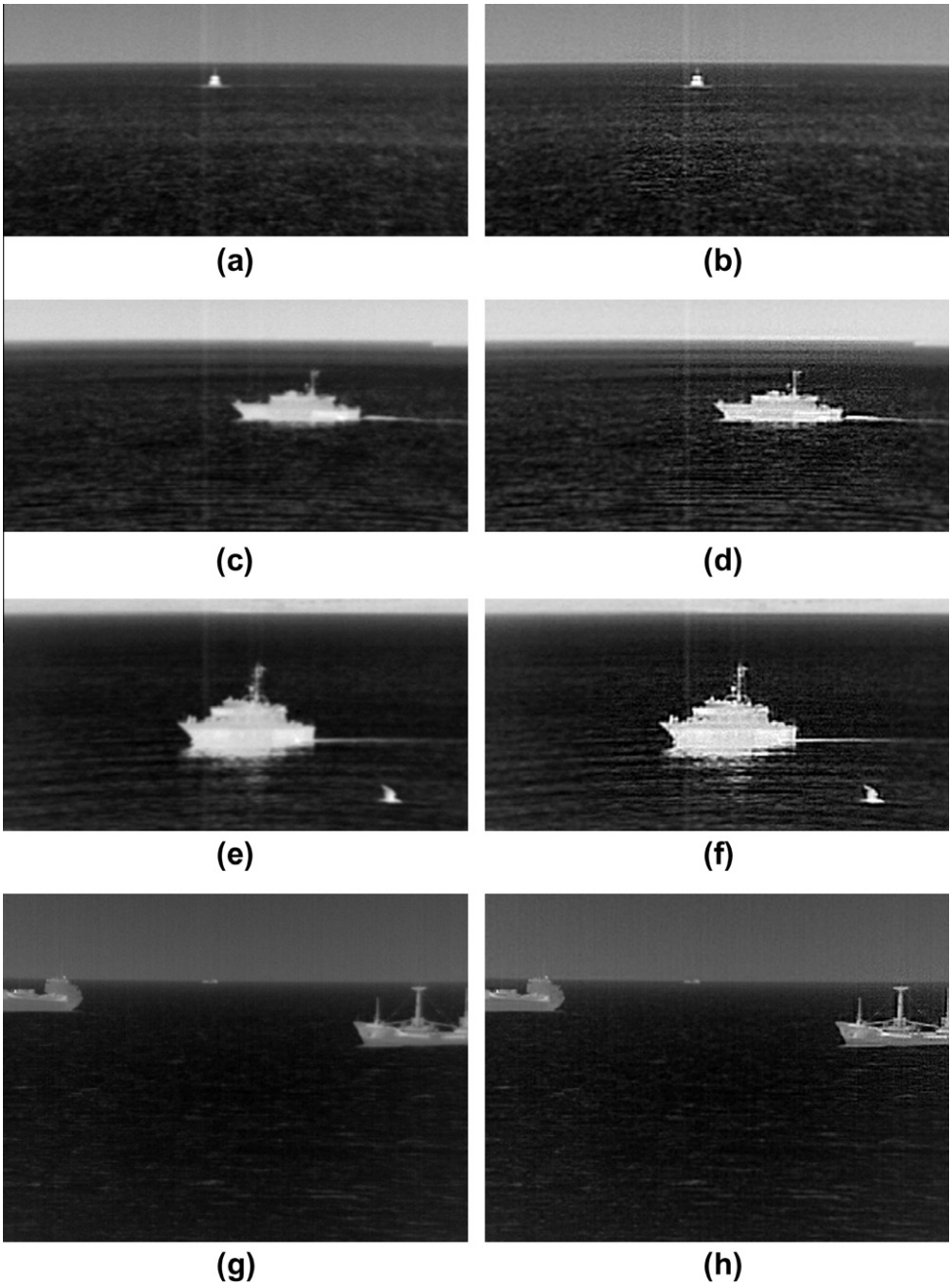

Fig. 15. Enhancement results for the different scenarios.

Here, p determines the degree of nonlinearity, n is the noise related parameter, and s is a member of the set $\{LH, HL\}$. Enhancement results obtained for each algorithm with the original image are given in Figs. 16 and 17, for the image sizes of [136,272] and [240,320], respectively. Results show that global contrast enhancement algorithms increase the clutter and noise levels in the background regions and target detail enhancement is limited to avoid this fact. As seen in Figs. 16e and 17e, AEMCWC increases target details more with less concerns about the clutter and noise when compared to the other methods.

5.1. Subjective tests

In the subjective tests, a similar way like in the study [9] is followed. Twenty observers (12 men and 8 women) having an average age of 28.5 and at least undergraduate degrees are asked to give points to the five different images based on the five different criteria. The criteria are the truthfulness of the image, detail visibility of the target and the background, unnatural artifacts, and total image quality. Each image appears randomly three times in the sequence, where a total of $5 \times 6 \times 3 = 90$ images are observed in a controlled office environment. In the evaluation, no information is given to the observers about the methods implemented and the original image. In the implementation, the tunable variables are determined by many trials and set to constants as they do not significantly vary for the images of similar characteristics in our database. In the implementation, the parameters of the algorithms AEMLFC, BCLAHE-CE, and MAM are set as in [30]. In the AEMCWC, number of cluster c is taken as 20 and other parameters are set as $\alpha_1 = 4$, $\alpha_2 = 1$, $\alpha_3 = 0.1$, $\alpha_4 = 0.1$, $\beta_1 = 1$, $\beta_2 = 1.5$, $\beta_3 = 1$, and

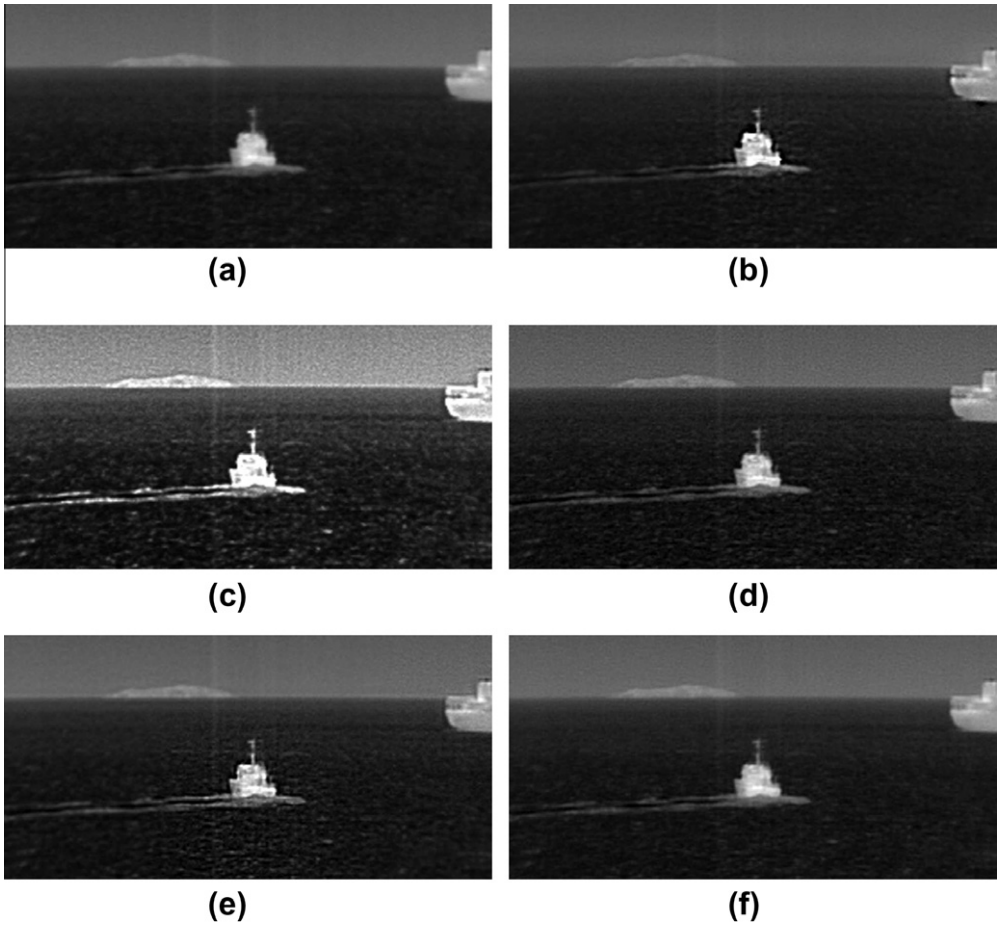

Fig. 16. Comparison results: (a) original image and enhanced images of size [136,272] for: (b) AEMLFC, (c) BCLAHE-CE, (d) MAM, (e) AEMCWC, and (f) WEM.

$\beta_4 = 1$. In the implementation of the WEM algorithm, p, n, and γ are taken as 0.5, 30, and 100.

Mean scores of the observers and associated 95% confidence intervals are given in Table 2. In the evaluation, AEMCWC has taken the highest points in the truthfulness, detail level in the target, in the artificiality, and in the total quality. The confidence intervals for AEMCWC show that the scores do not diverge much from the mean. In the background detail, BCLAHE-CE is slightly better than AEMCWC. Greatest score difference is observed in the total quality between the AEMCWC and other methods. AEMCWC provides target detail enhancement without introducing artificial effects as seen in the subjective evaluations. The results are also consistent with our previous work [30] where AEMLFC shows better performance in the target detail when the proposed algorithm is excluded in the evaluation.

5.2. Computational cost of the algorithms

The average computational cost of the algorithms used in the evaluations are given in Table 3 for the two different cameras. The algorithms are implemented using MATLAB version 7.5 on a Pentium PC with a Core 2 Quad CPU of 2.8 GHz and 3.25 GB Ram running on Microsoft XP SP3 operating system. MAM is the fastest algorithm among the methods compared with the average times of 0.02 and 0.03 s for the image sizes of [136,272] and [240,320], respectively. WEM is the second fast algorithm. AEMCWC method is better than AEMLFC in terms of operation speed. As the image size changes from [136,272] to [240,320], the increase in the processing time is dramatic in the AEMLFC and BCLAHE-CE. The average processing time for AEMCWC is about 1.1 s and does not show large variations as the size of the image increases.

6. Conclusions and future work

In this study, we proposed a content-based IR-IE method based on clustering of wavelet coefficients. In IE, the proposed solutions are case dependent; therefore it is very difficult to develop an enhancement technique working well under different conditions. We turn our attention to develop an enhancement technique for sea-surveillance system. Enhancement result of our method is compared with other IE techniques through subjective tests. The proposed algorithm outperforms other promising algorithms in the truthfulness, detail visibility of the target, artificiality, and total quality criteria in the subjective evaluations. We also compared the computational cost of the algorithms and found the processing time of the proposed method fair enough for real time applications.

Although we have concentrated on the enhancement of sea surface targets, the results can be easily expanded to other IR images consisting of similar target and background region discrimination in terms of wavelet coefficient distributions. Region based enhancement proposed in this study gives the possibility of enhancing IR images with less concerns about the enhancement of background noise and clutter.

The parameters of the method should be refined for specific scenarios in the operational environment. The user can adjust these parameters controlling truthfulness, target detail, background detail, artificiality, and total quality criteria to achieve the desired

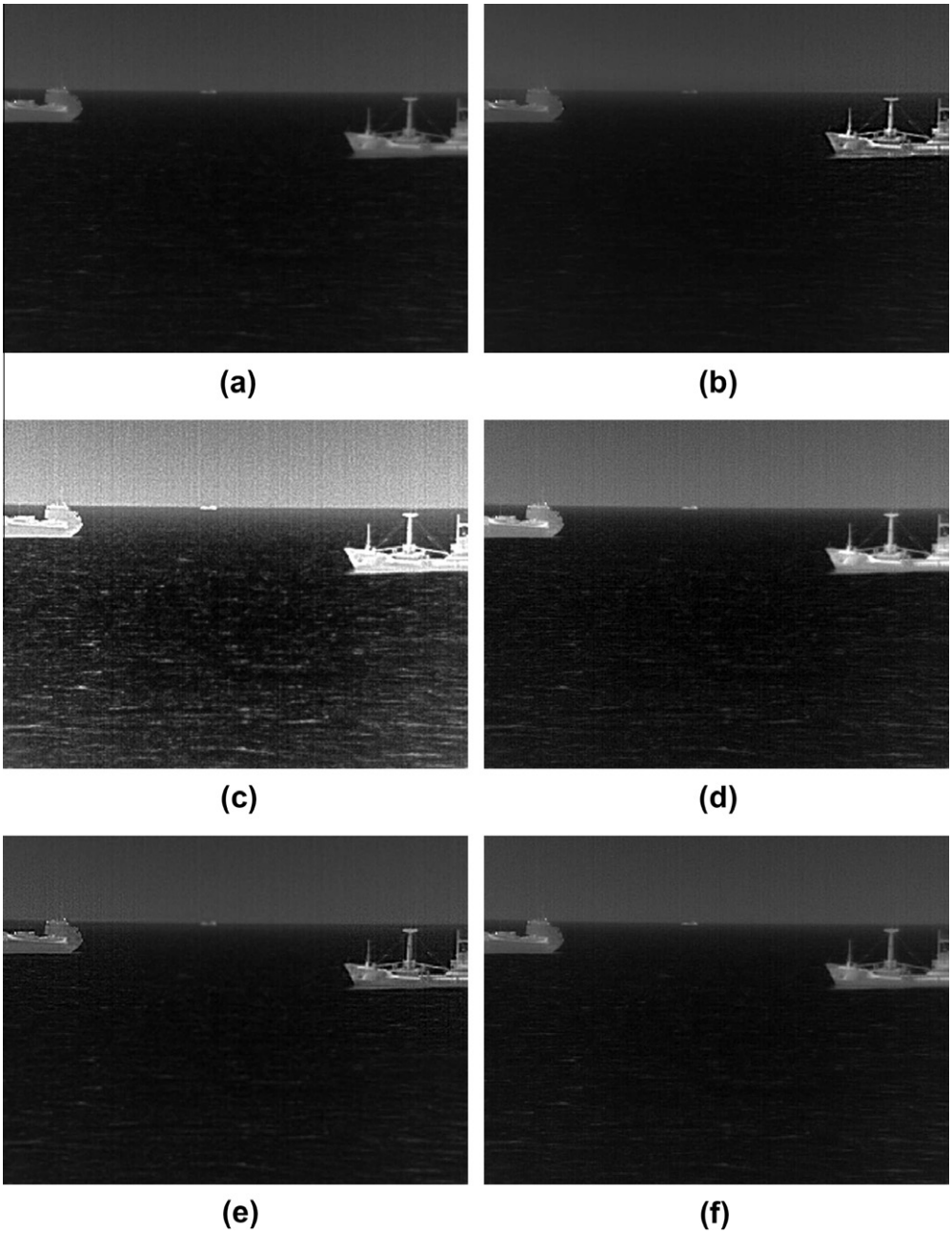

Fig. 17. Comparison results: (a) original image and enhanced images of size [240,320] for: (b) AEMLFC, (c) BCLAHE-CE, (d) MAM, (e) AEMCWC, and (f) WEM.

Table 2
Mean scores and 95% confidence intervals (in the brackets) of the observers (1: bad, 2: poor, 3: fair, 4: good, and 5: excellent).

	Original image	AEMLFC	BCLAHE-CE	MAM	AEMCWC	WEM
Truthfulness	2.63 [2.54,2.72]	2.87 [2.77,2.96]	2.62 [2.51,2.72]	3.01 [2.91,3.11]	**3.17** [3.07,3.28]	2.87 [2.78,2.96]
Target detail	2.21 [2.11,2.32]	3.21 [3.10,3.32]	2.74 [2.60,2.87]	3.01 [2.89,3.13]	**3.34** [3.22,3.47]	2.59 [2.47,2.71]
Background detail	2.26 [2.17,2.35]	2.51 [2.40,2.61]	**3.08** [2.96,3.20]	2.90 [2.79,3.01]	2.92 [2.81,3.03]	2.53 [2.43,2.63]
Artificiality	2.61 [2.51,2.71]	2.82 [2.72,2.91]	2.56 [2.45,2.66]	2.96 [2.86,3.06]	**3.05** [2.95,3.16]	2.80 [2.70,2.89]
Total quality	2.41 [2.32,2.50]	2.90 [2.81,2.99]	2.69 [2.58,2.79]	3.01 [3.00,3.02]	**3.21** [3.11,3.31]	2.75 [2.65,2.84]

enhancement in the practical application. In future studies, these parameters can be optimized using synthetic images including different sea platform models captured at different atmospheric conditions and sea surface reflections.

The proposed algorithm can also be accompanied with the existing wavelet-based target detection techniques in IR imaging systems. While we have concentrated on IR imaging in longwave, the technique proposed and compared with other methods in this paper may be useful for other IR wavelength intervals and also in visible band with the necessary tuning of the parameters. We also plan to implement the proposed algorithm in hardware using field programmable gate arrays for real-time processing.

Table 3
Average computational cost of the algorithms in seconds for the images used in the subjective evaluations.

	Image	Size
Enhancement methods	[136,272]	[240,320]
AEMLFC	1.94	6.76
BCLAHE-CE	1.02	19.86
MAM	**0.02**	**0.03**
AEMCWC	1.00	1.32
WEM	0.24	0.30

Acknowledgments

The authors thank Dr. M. Alper Kutay and Dr. S. Gökhun Tanyer for their supports in this study, Dr. Ö. Nezih Gerek for many helpful discussions and suggestions, and the observers for joining in the subjective evaluations.

References

[1] C.R. Zeisse, C.P. McGrath, K.M. Littfin, H.G. Hughes, Infrared radiance of the wind-ruffled sea, Journal of the Optical Society of America A 16 (1999) 1439–1452.
[2] W.K. Pratt, Digital Image Processing, Wiley, 2001.
[3] T. Pace, D. Manville, H. Lee, G. Cloud, J. Puritz, A multiresolution approach to image enhancement via histogram shaping and adaptive Wiener filtering, in: S.E.R.Z. Rahman, M.A. Neifeld (Eds.), Proceedings of the SPIE Visual Information Processing XVII, vol. 6978, 2008, pp. 1–11.
[4] R. Eschbach, K.T. Knox, Error-diffusion algorithm with edge enhancement, Journal of the Optical Society of America A 8 (1991) 1844–1850.
[5] R. Highnam, M. Brady, Model-based image enhancement of far infrared images, IEEE Transactions on Pattern Analysis and Machine Intelligence 19 (1997) 410–415.
[6] M. Tang, S. Ma, J. Xiao, Model-based adaptive enhancement of far infrared image sequences, Pattern Recognition Letters 21 (2000) 827–835.
[7] U. Qidwai, Infrared image enhancement using H_∞ bounds for surveillance applications, IEEE Transactions on Image Processing 17 (2008) 1274–1282.
[8] R.R. Muise, A. Mahalanobis, Image enhancement for automatic target detection, in: F.A. Sadjadi (Ed.), Proceedings of the SPIE Automatic Target Recognition XII, vol. 4726, 2002, pp. 267–272.
[9] F. Branchitta, M. Diani, G. Corsini, A. Porta, Dynamic-range compression and contrast enhancement in infrared imaging systems, Optical Engineering 47 (2008). 076401:1–14.
[10] R. Fattal, D. Lischinski, M. Werman, Gradient domain high dynamic range compression, in: Proceedings of the 29th Annual Conference on Computer Graphics and Interactive Techniques, ACM Press, 2002, pp. 249–256.
[11] B. Funt, F. Ciurea, J. McCann, Retinex in MATLAB, Journal of Electronic Imaging 13 (2004) 48–57.
[12] F. Branchitta, M. Diani, G. Corsini, M. Romagnoli, New technique for the visualization of high dynamic range infrared images, Optical Engineering 48 (2009) 1–9.
[13] R. Lai, Y. Yang, B. Whang, H. Zhou, A quantitative measure based infrared image enhancement algorithm using plateau histogram, Optics Communications 283 (2010) 4283–4288.
[14] C.-L. Lin, An approach to adaptive infrared image enhancement for long-range surveillance, Infrared Physics and Technology 54 (2011) 84–91.
[15] X. Bai, F. Zhou, Hit-or-miss transform based infrared dim small target enhancement, Optics and Laser Technology 43 (2011) 1084–1090.
[16] X. Bai, F. Zhou, B. Xue, Infrared image enhancement through contrast enhancement by using multiscale new top-hat transform, Infrared Physics and Technology 54 (2011) 61–69.
[17] T. Yu, Q. Li, J. Dai, New enhancement of infrared image based on human visual system, Chinese Optics Letters 7 (2009) 206–209.
[18] G. Deng, A Generalized unsharp masking algorithm, IEEE Transactions on Image Processing 20 (2011) 1249–1261.
[19] P. Shanmugavadivu, K. Balasubramanian, Image edge and contrast enhancement using unsharp masking and constrained histogram equalization, in: Communications in Computer and Information Science: Control, Computation and Information Systems, vol. 140, Springer, Berlin Heidelberg, 2011, pp. 129–136.
[20] E. Salari, Z. Ling, Texture segmentation using hierarchical wavelet decomposition, Pattern Recognition 28 (28) (1995) 1819–1824.
[21] R. Larsen, M.B. Stegmann, S. Darkner, S. Forchhammer, T.F. Cootes, B.K. Ersbøll, Texture enhanced appearance models, Computer Vision and Image Understanding 106 (1) (2007) 20–30.
[22] C. Hsieh, E. Lai, Y. Wang, An effective algorithm for fingerprint image enhancement based on wavelet transform, Pattern Recognition 36 (2003) 303–312.
[23] J. Tang, X. Liu, Q. Sun, A direct image contrast enhancement algorithm in the wavelet domain for screening mammograms, IEEE Journal of Selected Topics in Signal Processing 3 (2009) 74–80.
[24] N. Unaldi, S. Temel, V.K. Asari, Z. Rahman, An automatic wavelet-based nonlinear image enhancement technique for aerial imagery, in: Proceedings of the IEEE 4th International Conference on Recent Advances in Space Technologies, 2009, pp. 307–312.
[25] Y. Wan, D. Shi, Joint exact histogram specification and image enhancement through the Wavelet transform, IEEE Transactions on Image Processing 16 (2007) 2245–2250.
[26] D. Heric, B. Potocnik, Image enhancement by using directional wavelet transform, Journal of Computing and Information Technology 4 (2006) 299–305.
[27] M. Shao, G. Liu, X. Liu, D. Zhu, A new approach for infrared image contrast enhancement, in: J.C.W.H.W.X. Hou, J. Yuan, S. Han (Eds.), Proceedings of the SPIE 2nd International Symposium on Advanced Optical Manufacturing and Testing Technologies: Optical Test and Measurement Technology and Equipment, vol. 6150, 2006, pp. 1–6.
[28] R.N. Strickland, H.I. Hahn, Wavelet transform methods for object detection and recovery, IEEE Transactions on Image Processing 6 (1997) 724–735.
[29] C.J. Zhang, X.D. Wang, Typhoon cloud image enhancement and reducing speckle with genetic algorithm in stationary wavelet domain, IET Image Processing 3 (4) (2009) 200–216.
[30] A.O. Karalı, O.E. Okman, T. Aytaç, Adaptive enhancement of sea-surface targets in infrared images based on local frequency cues, Journal of the Optical Society of America A 27 (2010) 509–517.
[31] S. Weith-Glushko, C. Salvaggio, Quantitative analysis of infrared contrast enhancement algorithms, in: G.C. Holst (Ed.), Proceedings of the SPIE Infrared Imaging Systems: Design, Analysis, Modeling, and Testing XVII, vol. 6543, 2007, pp. 1–12.
[32] A. Polesel, G. Ramponi, V.J. Mathews, Image enhancement via adaptive unsharp masking, IEEE Transactions on Image Processing 9 (2000) 505–510.
[33] R.O. Duda, P.E. Hart, D.G. Stork, Pattern Classification, John Wiley & Sons, New York, 2001.
[34] K.V. Velde, Multiscale color image enhancement, Proceedings of the IEEE International Conference on Image Processing 3 (1999) 584–587.